https://doi.org/10.5194/acp-2022-473
Preprint. Discussion started: 28 July 2022

Atmospheric Chemistry and Physics Discussions

Aerosol first indirect effect of African smoke in marine stratocumulus clouds over Ascension Island, south Atlantic Ocean

Martin de Graaf[1], Karolina Sarna[2], Jessica Brown[3], Elma Tenner[2], Manon Schenkels[4], and David P. Donovan[1]

[1]Royal Netherlands Meteorological Institute (KNMI) R&D Satellite Observations, De Bilt, The Netherlands
[2]Geosciences & Remote Sensing Department, Delft University of Technology (TUD), Delft, The Netherlands
[3]Wageningen University, Meteorology and Air Quality Department, Wageningen, The Netherlands
[4]Utrecht University, Institute for Marine and Atmospheric Research, Utrecht, The Netherlands

Correspondence: M. de Graaf, martin.de.graaf@knmi.nl

Abstract.

The first indirect or Twomey effect was measured in marine stratocumulus clouds over the south Atlantic Ocean. Measurements were collected over Ascension Island, a remote spot between the African and South American continents. This area is known for its persistent broken cloud cover and smoke intrusions from vegetation fires in Africa during the monsoonal dry period. The interactions between aerosols and clouds are among the least understood climatic processes and were studied over Ascension using a combination of in-situ and remote sensing instruments. Particularly, a new method using a ground-based UV-polarisation lidar to infer cloud droplet sizes and droplet number concentrations was tested against more traditional radar-radiometer measurements. The lidar measurements show to be robust and at least as accurate as the lidar-radiometer measurements and have the large advantage of depending on a single instrument. The UV-lidar was deployed on Ascension for one month in the summer of 2016 and one month in the summer of 2017. In 2016, the presence of smoke in the troposphere decreased the effective cloud droplet size and increased the average droplet number distribution. In 2017, alignment problems of the lidar prohibited conclusions about a Twomey effect. The cloud microphysical properties showed differences between the two years depending on the meteorological circumstances.

1 Introduction

The typical clouds found in subtropical marine regions, such as around Ascension Island, are low lying bands of stratocumulus capping the boundary layer, typically found between 1-1.5 km. These marine stratocumulus clouds are very important for the global climate, as they have a high albedo compared to the dark ocean over which they occur and reflect around 30% of the incoming solar radiation (Bennartz, 2007). An estimated 4% increase in their cover could offset the warming due to a doubling of CO2 (Albrecht et al., 1988). These clouds are associated with large-scale subsidence over a cool ocean (Paluch et al., 1991).

https://doi.org/10.5194/acp-2022-473
Preprint. Discussion started: 28 July 2022


Atmospheric Chemistry and Physics Discussions

Such conditions lead to a strong temperature inversion at the top of the boundary layer, through which clouds are not able to penetrate, leading to expansive decks of stratocumulus clouds. They are maintained by turbulent mixing due to longwave cooling at the cloud top and sustained by a balance between moisture supply from the ocean surface and the entrainment of dry air from the troposphere (Bennartz, 2007). This longwave cooling at the cloud top also enhances the strength of the inversion layer (Paluch et al., 1991). They are typically accompanied by light drizzle. As these clouds are so important in modulating the Earth's climate, any interactions which they have with aerosols are also very important in regulating the earth-atmosphere system.

In this paper, a method is explored to study the impact of light absorption by natural smoke excursions in, under and over the stratocumulus cloud deck on the development of the cloud deck, using one single instrument, a UV-polarisation lidar. Such an instrument was located on Ascension Island, a remote island in the south Atlantic Ocean, for one month in 2016 and one month in 2017 during the dry season in Africa, when numerous vegetation fires annually produce smoke which is often transported over the Atlantic. The UV-lidar measurements were part of the measurement campaign CLARIFY-2017 (Haywood et al., 2021), partnering with the LASIC (Zuidema et al., 2016), ORACLES (Redemann et al., 2020) and AEROCLO-sA (Formenti et al., 2019) campaigns. The lidar data are used to derive both Aerosol Optical Thickness (AOT) from aerosol layers when present, and cloud parameters from the stratocumulus cloud deck. For the latter, a newly developed technique to infer cloud parameters based on polarisation change due to multiple scattering in clouds was tested (Donovan et al., 2015). The details of the retrievals of the aerosol and cloud properties are described in Sect. 2.

A short overview of the measurement campaign is given in Sect. 3. The measurements in 2017 were affected by alignment problems, which resulted in a lower SNR compared to the 2016 measurements. Therefore, the measurements from 2016 are used mainly to show the Twomey effect in the stratocumulus clouds. The consistency of the lidar measurements was investigated by comparing with the abundant additional campaign measurements, which is described in Sect. 4.

2 Theory

2.1 UV-lidar

The total power returned to a lidar by backscattering in the atmosphere under single scattering conditions is

$$P(z) = \frac{C_{\mathrm{lid}}}{z^2}\beta_\pi(z)\exp\left(-2\int_0^z \alpha(z')dz'\right) \tag{1}$$

where P is the power received by the instrument, z the altitude from the instrument along the line of sight, C_{lid} a lidar calibration coefficient, α the atmospheric extinction coeffient, and β_π the atmospheric backscatter coefficient. The atmospheric extinction and backscatter coefficients can be devided into a molecular, aerosol, and cloud part, viz.

$$\begin{aligned}\alpha &= \alpha_{\mathrm{m}} + \alpha_{\mathrm{a}} + \alpha_{\mathrm{c}} \\ \beta_\pi &= \beta_{\mathrm{m}} + \beta_{\mathrm{a}} + \beta_{\mathrm{c}}\end{aligned} \tag{2}$$

https://doi.org/10.5194/acp-2022-473
Preprint. Discussion started: 28 July 2022

Atmospheric Chemistry and Physics Discussions

The extinction-to-backscatter ratio, or lidar ratio, S is defined as $S(z) = \alpha/\beta$. The aerosol scattering ratio (R_{asca}) is defined as $R_{\mathrm{asca}} = (\beta_{\mathrm{a}} + \beta_{\mathrm{m}})/\beta_{\mathrm{m}}$, which is 1 if there are no aerosols.

2.2 Molecular scattering

The molecular backscatter coefficient can be calculated using (Collis and Russel, 1976)

$$\beta_{\mathrm{m}} = \frac{\rho_{\mathrm{atm}}}{M}\left(\frac{\lambda}{550}\right)^{-4.09} 10^{-32}\ \mathrm{m}^{-1}\mathrm{sr}^{-1}, \tag{3}$$

where λ is the wavelength, M is the average molecular mass of air ($4.81 \cdot 10^{-26}$ kg), and the atmospheric density was determined using

$$\rho_{\mathrm{air}} = \frac{p}{T}\frac{1}{\rho_{\mathrm{dry\,air}}}, \tag{4}$$

where p is the measured pressure, T the measured temperature and $\rho_{\mathrm{dry\,air}}$ the gas density of dry air with an average value of $287 J\,kg^{-1}K^{-1}$. The temperature and pressure were determined from radiosondes, launched four times daily from Ascension Island. The molecular extinction coefficient α_m can be calculated using the molecular extinction-to-backscatter ratio S_{mol} = $8\pi/3$ sr (Guzzi, 2008).

At the lidar wavelength of 355 nm molecular scattering is strong and this was used to calibrate the lidar. Details can be found in Schenkels (2018).

2.3 AOT retrieval

If one of the components in Eq. (2) can be neglected, e.g. in a cloud-free atmosphere, where $\alpha_{\mathrm{c}} = 0$, $\beta_{\mathrm{c}} = 0$), or inside the cloud where $\alpha_{\mathrm{a}} \ll \alpha_{\mathrm{c}}$, $\beta_{\mathrm{a}} \ll \beta_{\mathrm{c}}$, the classical two-mode method following Klett (1981) and Fernald (1984) can be applied using transformed variables (Sarna et al., 2021)

$$P'(z) = S(z)P(z)\exp\left(2\int_0^z \alpha_m(z') - S(z')\beta_m(z')dz'\right) \tag{5}$$

and

$$\alpha'(z) = \left(S(z)\beta_m(z) + \alpha_a(z)\right). \tag{6}$$

Now Eq. (1) can be rewritten as

$$P'(z) = \frac{C_{lid}}{z^2}\alpha'(z)\exp\left(-2\int_0^z \alpha'(z')dz'\right), \tag{7}$$

with the analytical solution

https://doi.org/10.5194/acp-2022-473
Preprint. Discussion started: 28 July 2022

Atmospheric Chemistry and Physics Discussions

$$\alpha'(z) = \left[\frac{\frac{P'(z)z^2}{P'(z_0)z_0^2}}{\frac{1}{\alpha'(z_0)} + 2\int_z^{z_0} \frac{P'(z)z^2}{P'(z_0)z_0^2} dz'} \right]. \quad (8)$$

where z_0 is a normalisation height. From the transformed variable α' the aerosol extinction is derived to be $\alpha_a(z) = \alpha'(z) - S(z)\beta_m(z)$. The aerosol backscatter coefficient is now derived by dividing the aerosol extinction by the height dependent lidar ratio. The aerosol optical thickness (τ) of a layer can be obtained by integrating the aerosol extinction profile over the altitude of the layer:

$$\tau(z_1; z_2) = \int_{z_1}^{z_2} \alpha_a(z) dz \quad (9)$$

2.3.1 Cloud-free scenes

In clear sky scenes the normalisation height is set to an altitude at which the aerosol extinction is zero. From literature (e.g. Wandinger et al., 2016; Greatwood et al., 2017) and from observations on the island, it was concluded that marine aerosols are always present in the lower boundary layer, up until 1200 m. S_{marine} was set to be 25 sr, a good approximation for marine aerosols (Wandinger et al., 2016; Cattrall et al., 2005; Müller et al., 2007). (Aged) smoke and dust were often, almost always, present above the boundary layer, in the layer from 1200 m to 5000 m, sometimes mixed in the boundary layer. For this layer the lidar ratio S_{dark} was set to 50 sr (Wandinger et al., 2016). Above 5000 m, the air was mostly clean and clear of aerosols and the lidar ratio reduces to the molecular extinction-to-backscatter ratio defined above. The normalisation height was set to 7 km. Various tests were performed varying S_{marine} and S_{dark} around their values of 25 and 50 sr to check the sensitivity of the choices.

2.3.2 Aerosol below clouds

In order to derive aerosol optical thickness close to clouds, aerosol extinction profiles were retrieved for cloudy scenes under the clouds, using Eq. (8). However, in this case the normalisation height is not located at an altitude without aerosols, but inside the cloud where the aerosol contribution can be neglected. The normalisation height was determined by the cloud base height and the cloud extinction. The extinction-to-backscatter ratio was set to 20 sr in the cloud and 50 sr below the cloud (Wandinger et al., 2016).

Furthermore, multiple scattering, which influences the lidar return and the cloud extinction, should be taken into account in a cloud. Therefore, the cloud extinction-to-backscatter ratio, used to determine α' in Eq. (8), was corrected by a multiple scattering correction factor η

$$S_c = \frac{(1-\eta)\alpha_c}{\beta_c}. \quad (10)$$

The correction factor η was determined from a sensitivity study over three days in 2016 with broken clouds. Aerosol profiles below clouds during these days were fitted to aerosol retrievals during clear sky spells close in time on these days. The

https://doi.org/10.5194/acp-2022-473
Preprint. Discussion started: 28 July 2022

Atmospheric Chemistry and Physics Discussions

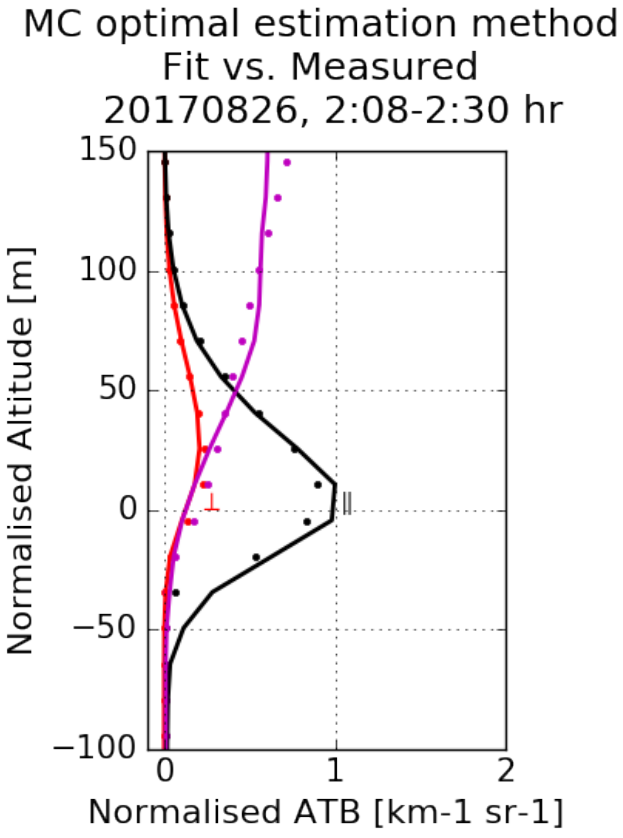

Figure 1. Measured (solid line) and fitted (dots) vertical profiles for the parallel attenuated backscatter (black), perpendicular attenuated backscatter (red) and depolarisation ratio (magenta) on 27 Aug. 2017.

correction factor was varied between 0.3 and 0.5 in steps of 0.05, resulting in overcorrection and undercorrection. The best fit was found for 0.35 and 0.4. The difference in aerosol extinction coefficient at an altitude of 300 m below cloud base between η = 0.35 and 0.4 is about $2.6 \cdot 10^{-5}$ m^{-1}. In all subsequent processing a value of η = 0.4 was used. See Tenner (2017) for details.

2.4 Clouds

Although the lidar equation (1) formally only applies for single scattering, the derivation of cloud extinction and backscatter coefficient in this section is based on a polarisation change after multiple scattering, first developed by Donovan et al. (2015). Light returning from a liquid cloud will be partially depolarised due to multiple scattering by the cloud droplets (Liou and Schotland, 1971). This multiple scattering in a liquid water cloud can be simulated by a Monte Carlo (MC) model, assuming a proper cloud model. This was achieved using the Earth Clouds and Aerosol Radiation Explorer (EarthCARE) simulator (ECSIM) lidar-specific MC forward model. The ECSIM lidar MC model is a modular multi-sensor simulation framework, which was used to calculate the spectral-polarisation state of the lidar signal.

https://doi.org/10.5194/acp-2022-473
Preprint. Discussion started: 28 July 2022

Atmospheric Chemistry and Physics Discussions

For the simulations, liquid water clouds with a (quasi-)linear liquid water content (LWC) and a (quasi-)constant cloud droplet number concentration (N_d) were assumed (e.g. de Roode and Los, 2008). The cloud droplet size distribution was defined as a single-mode modified-gamma distribution (Miles et al., 2000)

$$n(r) = \frac{N_d}{R_m} \frac{1}{(\gamma - 1)!} \left(\frac{r}{R_m} \right)^{\gamma - 1} \exp\left(\frac{r}{R_m} \right), \tag{11}$$

where N_d is the cloud droplet concentration, defined to be constant with height, r is the droplet radius, R_m the mode radius and γ the shape parameter of the distribution.

A linear liquid water content defines a constant liquid water lapse rate, Γ_l. When the liquid water content increases with height and the number density remains constant, the cloud droplet effective radius, defined as

$$R_{\text{eff}} = \frac{\int n(r) r^3 dr}{\int n(r) r^2 dr}, \tag{12}$$

will increase with height. The cloud extinction coefficient, α_c, also increases with height. This leads to the prediction that the depolarisation ratio is generally increasing throughout the cloud, while observations show that the depolarisation ratio may exhibit a peak (Sassen and Petrilla, 1986). Furthermore, the model represents semi-infinite clouds, with a cloud top at infinity. However, the lidar signal can only penetrate a few hundred meters into the cloud. Therefore, no information is known about the upper part of the cloud and any retrieved parameters are only applicable to the cloud-base region and the parameters were calculated for a reference height. In this research, 100 m above cloud-base was assumed. This simple but effective cloud representation reduces the parameters to describe the cloud to two, the cloud extinction α_c^{100} at reference height, and the cloud effective radius R_{eff}^{100} at reference height.

MC simulations were performed for various values of the cloud base height (CBH), the lidar field-of-view (FOV), R_{eff}^{100} and Γ_l. The values are replicated from (Donovan et al., 2015) in Table 1. Look-up tables (LUTs) were generated from the simulations and predefined input parameters, the lidar constants and initial values for R_{eff}^{100} and α_c^{100}. These LUTs contain information on the simulated parallel and perpendicular attenuated backscatter and therefore the depolarisation ratio.

The observed attenuated backscatter and depolarisation ratio were compared to the LUTs to find the best matching values for R_{eff}^{100} and α_c^{100}, by iteratively minimizing a cost-function (Rodgers, 2000). In Fig. 1, the observed and fitted attenuated backscatter profiles from the LUTs are shown, for a cloud selected on 26 August 2017. The dotted lines correspond to the fitted

Table 1. Range of parameters used in the ECSIM MC calculations

Parameter	Values
CHB[km]	0.5,1.0,2.0,4.0
FOV[mrad]	0.5,1.0,2.0,4.0
R_{eff}^{100} [μm]	2.0,2.6,3.3,4.3,5.6,7.2,9.3,12.0
Γ_l[g m^{-3} km^{-1}]	0.1,0.2,0.4,0.6,0.8,1.0,1.2,1.4,1.6,1.8,2.0

https://doi.org/10.5194/acp-2022-473
Preprint. Discussion started: 28 July 2022


Atmospheric Chemistry and Physics Discussions

values from the LUTs, with the parallel attenuated backscatter in black, the perpendicular attenuated backscatter in red and the depolarisation ratio in magenta. The observed profiles are represented by the corresponding solid lines.

The cloud drop number density ND follows from the cloud effective radius and the cloud extinction

$$ND = \alpha_c^{100} \frac{1}{2\pi} \frac{1}{(R_{\text{eff}}^{100})^2} \frac{1}{k}, \tag{13}$$

where k is 0.75 ± 0.15.

Because multiple-scattering occurs in a cloud, the LUTs, the shape of the attenuated backscatter and the depolarisation ratio profiles are all well-defined functions of the LWC and effective radius profile. For single-scattering the parallel attenuated backscatter profile will not depend on the effective radius profile.

It is important to note that the CBH is difficult to define from real observation due to the presence of sub-cloud drizzle and the presence of growing aerosol particles. The MC based inversion results would be very sensitive to the absolute calibration of the attenuated backscatter if the CBH is used as a reference. Therefore, the peak of the observed parallel lidar attenuated backscatter is used as a reference instead of the CBH in the fitting procedure. Consequently, the CBH is produced as a by-product and in Sect. 4 the derived CBH will be compared to observations of the CBH using different instruments.

2.5 Aerosol-Cloud interaction

The most straightforward aerosol-cloud interaction is the change in cloud droplet number due to a change in the number of available condensation nucleii for a constant ambient relative humidity, the first indirect or Twomey effect (Twomey, 1977). In order to quantify this effect, the Indirect Effect (IE) parameters defined by Feingold et al. (2001) were used, to describe the relative change of cloud properties against the relative change in aerosols A. For the cloud effective radius

$$\text{IE}_r = -\frac{d\ln R_{\text{eff}}}{d\ln A}. \tag{14}$$

For the cloud droplet number density

$$\text{IE}_N = -\frac{d\ln ND}{d\ln A}. \tag{15}$$

In these equations A is the aerosol proxy, which should represent the aerosol abundance, and can be aerosol extinction, aerosol optical thickness or another aerosol quantity.

3 Measurement campaign

From 1–30 September 2016 and from 15 August to 9 September 2017 the KNMI UV-polarisation lidar, normally located in Cabauw, The Netherlands, was relocated to Ascension Island, a remote volcanic island in the tropical Atlantic Ocean (8°S,14°W). Ascension Island is located 1600 km from the African coast and 2250 km from the Brazilian coast. Its climate is a tropical desert, with temperatures ranging from 22 to 31°C and a low annual rainfall at an average of 142 mm (Dorman

https://doi.org/10.5194/acp-2022-473
Preprint. Discussion started: 28 July 2022

Atmospheric Chemistry and Physics Discussions

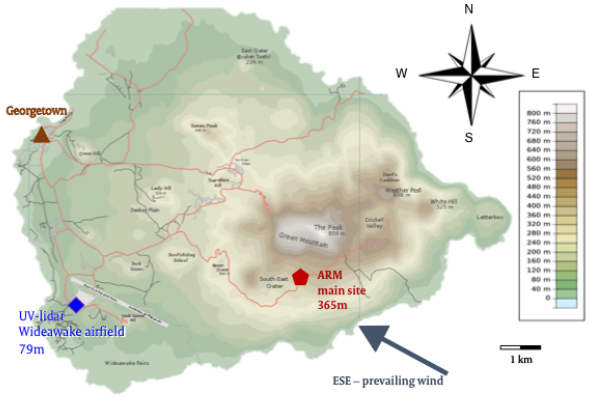

Figure 2. Map of Ascension Island, showing the topography and the location of the UV-lidar on Wideawake airfield and the ARM main site. The distance between the sites is 6.3 km. Georgetown is the island's main settlement.

and Bourke, 1981), the peak rainfall occurring in April. Typical clouds found in subtropical marine regions, such as around Ascension Island, are low lying bands of stratocumulus capping the boundary layer, found around 1–1.5 km altitude. The prevailing winds in the boundary layer are from the south east (Kim et al., 2003) and mostly invariant. Above the boundary layer ($>$ 1200 m above sea level) the wind is coming from the equatorial regions and are frequently loaded with suspended particles like smoke from African vegetation fires or desert dust.

The Ascension Island Initiative (ASCII) aimed at identifying microphysical properties of marine stratocumulus clouds in the presence of aerosols. Details of the measurement campaign can be found in Brown (2016); Tenner (2017); Schenkels (2018). During the same time various other measurements campaigns were operated on and around Ascension, providing a myriad of complementary measurements. The ground-based campaign LASIC (Zuidema et al., 2016) operated a fully-equipped ARM Research Facility during 2016 and 2017, while air-borne measurements were provided during 2017 by CLARIFY-2017 (Haywood et al., 2021), and in 2016, 2017, and 2018 by ORACLES (Redemann et al., 2020). On the African continent, in-situ and airborne measurements of the smoke near the source were provided by the AEROCLO-sA campaign in Namibia (Formenti et al., 2019).

Figure 2 shows the main locations of the instruments used in this paper during the campaigns. The UV-lidar was located on the southwest side of the island throughout the 2016 and 2017 campaigns on Wideawake airfield, at 79 m above sea level. All of 2016 and 2017 the ARM research facility was located on the south slope of Green Mountain, at 859 m the highest peak of the volcanic island. This location ensured the transport of pristine oceanic air at the prevailing wind direction, which is east-southeast. The ARM research facility was located at 365 m altitude and about 6 km from Wideawake airfield. Radiosondes were launched from the airfield four times daily.

4 Results

https://doi.org/10.5194/acp-2022-473
Preprint. Discussion started: 28 July 2022

Atmospheric Chemistry and Physics Discussions

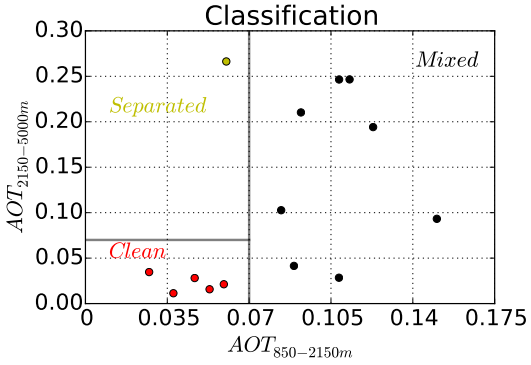

Figure 3. Classification of the average clear-sky AOT during broken cloud days, at two levels: from 850 to 2150 m, assumed to be at cloud level, and from 2150 to 5000 m, which is assumed to be in the free troposphere above the clouds.

4.1 Classification

A first coarse indication of the change in cloud properties can be obtained from a comparison of periods with a high aerosol loading over Ascension Island, compared to periods with low aerosol loading, assuming everything else will be the same. A classification was made using the 2016 measurements using the clear sky aerosol extinction retrievals, i.e. using Eqs. 8 and 9, after defining periods of clear sky and cloudy periods for each day with broken clouds and useful cloud property retrievals. The average aerosol optical thickness was determined during the cloud free periods, and the average cloud properties were determined during the cloudy periods.

A classification was made of days when aerosols were expected to mix with the clouds and days when the aerosol loading was particularly low. Figure 3 explains the logic: two layers were discriminated, one from 850 to 2150 altitude, which is assumed to be the altitude of the clouds, and from 2150 to 5000 m, which is the free troposphere. If the AOT in both layers was low (below 0.07 was chosen), the day was assigned the label ‘clean’, if the AOT in the layer between 850 and 2150 m was high (higher than 0.07), the days was assigned the label ‘mixed’. If the AOT was high only in the upper air, the day was labeled ‘separated’ and not considered, which happened in one case.

Using this crude selection of cases resulted in a clear difference in the average cloud properties between the different days, as shown in Fig. 4. ND was 294±91 cm^3 during all ‘clean’ days, doubling to over 611±191 cm^3 during the ‘mixed’ days. Conversely, R_{eff}^{100} was reduced from 3.81±0.6 μm to 2.85±0.2 μm. This suggests a change to smaller more numerous cloud particles with the availability of a larger number of cloud condensation nuclei. However, the assumption that the humidity does not change cannot be garantueed with such an approach.

4.2 AOT around cloud base

In order to determine the cloud properties and aerosol availability as close together in time as possible, two approaches are presented. First, by determining the AOT from the daily average extinction profile as before, but now averaged around the

https://doi.org/10.5194/acp-2022-473
Preprint. Discussion started: 28 July 2022

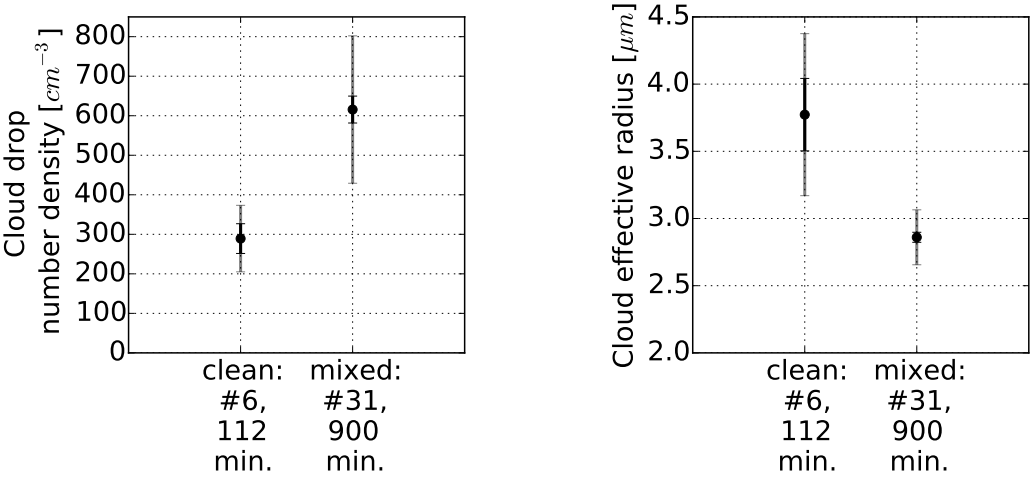

Figure 4. The mean value of the cloud droplet number density ND (left) and the cloud effective radius at reference height R_{eff}^{100} (right) for the 'clean' and 'mixed' cases. The black error bar represents the standard error of the mean, the grey bars represent the sample standard deviation.

cloud base, more specifically from 300 m below the cloud base until 1000 m above the cloud base. It is assumed that aerosols between these levels have a significant impact on cloud forming. For each cloudy period the cloud properties were determined and used in Eqs. (14) and (15) to quantify the indirect effect. The results are shown in Fig. 5.

A linear fit was drawn through the points, weighted by the standard deviation, showing the indirect effect: 0.3 ± 0.21 cm^{-3} for the cloud droplet number density and 0.18 ± 0.06 μm for the cloud effective radius.

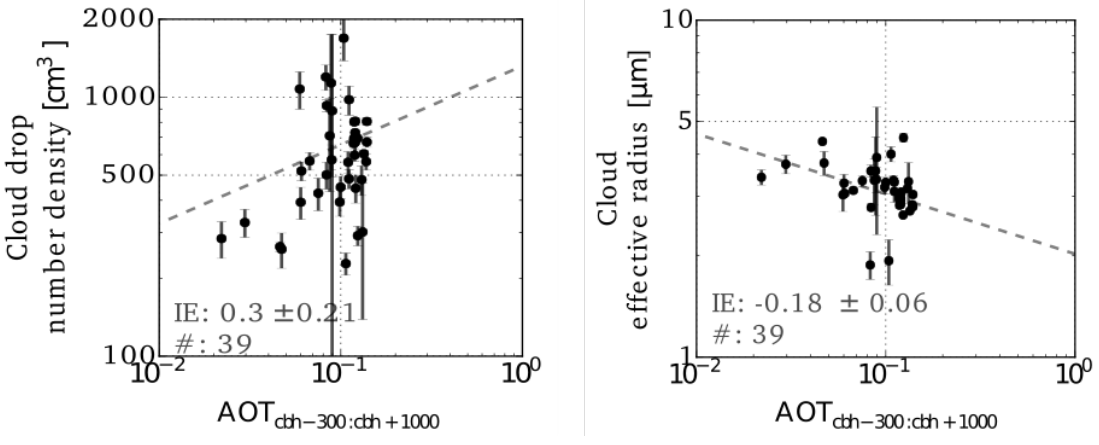

Figure 5. (Left) Weighted mean of the cloud drop number density versus daioly average AOT for each cloud selection. (Right) Weighted mean of the cloud effective radius versus daily average AOT for each cloud selection. For both cloud properties a linear fit is plotted and the Indirect Effect parameter (IE) is given. The standard error of the mean values were used as weights in the fit.

https://doi.org/10.5194/acp-2022-473
Preprint. Discussion started: 28 July 2022


Atmospheric Chemistry and Physics Discussions

4.3 AOT below the cloud

In order to get aerosol and cloud proxies closer together in time, IE_r and IE_N were also calculated using the AOT below the clouds during cloudy periods. For this, the aerosol extinction profile was computed using Eq. (8), but with the normalisation height set inside the cloud and the extinction-to-backscatter ratio set to 20 sr in the cloud and 50 sr below the cloud, as described in Sect. 2. Furthermore, the cloud extinction-to-backscatter ratio was corrected for multiple scattering (Eq. (10)). The extinction profile was determined from 200 m above the lidar, to avoid overlap, until 300 m below cloud base to avoid the mixing region of wet aerosols just below the cloud. The mean aerosol extinction coefficient was used instead of the AOT, because the height of the range bins changed per cloud selection.

For the cloud retrievals 30 s intervals were averaged, with a minimum of 3 values and a maximum of 24 values, corresponding to cloud periods of 1.5 to 12 minutes. The errors from the cloud inversion were used as weights in the determination of the IE-values. The results for the 2016 measurements are plotted in Fig. 6

The IE values for all cloud periods during the 2016 campaign show varying results. Many values are beyond the theoretically feasible values, indicated in the plots by the grey horizontal lines. Theoretically the absolute value of IE_N must be below 1 and the absolute value of IE_r below 0.33. However, a number of retrievals show much larger values, characterised by large uncertainties. The theoretical numbers are based on theoretical clouds in a constant atmospheric state. The retrievals with large numbers and large uncertainties must be associated with variable meteorological conditions that drive the changes in cloud and aerosol properties.

Around 12–15 August IE_N ranges from positive to zero, while IE_r ranges from -0.33 to zero. The same happens around 20–24 August. This may be indicative of a Twomey effect, which at some point saturates, i.e. after enough CCNs are available, no more smaller cloud droplets are formed. These episodes correspond to periods of elevated AOT over Ascension Island, see Fig. 7.

The three presented methods all suggest some indication of the Twomey effect in the stratocumulus clouds around Ascendion in 2016 during various episodes. However, the results are difficult to interpret due to the large senstivity of the retrieved AOT and cloud properties to various parameters and instrument noise. In 2017, no conclusive effect could be retrieved from the lidar measurements, mainly due to pointing errors in the instrument, resulting in a lower SNR (Schenkels, 2018). In the next sections, the accuracy of the retrieved AOT and cloud properties are investigated using additional instruments located on the island.

5 Validation

5.1 Aerosol Optical Thickness

The AOT retrieved from the lidar was compared to AERosol RObotic NETwork (AERONET) measurements from the station located on Ascension Island (at the ARM main site. AERONET offers quality-assured, cloud-screened automated direct sun measurements from ground-based, sun-tracking sunphotomers every 15 minutes at 8 wavelengths. The measurements at

https://doi.org/10.5194/acp-2022-473
Preprint. Discussion started: 28 July 2022


Atmospheric Chemistry and Physics Discussions

340 nm were used here. The AERONET AOT data at this wavelength have an uncertainty of 0.021, due to atmospheric pressure variations assuming a 3% maximum deviation from the mean surface pressure (Eck et al., 1999). The uncertainty of the lidar retrieval, taking into account the systematic error arising from the definition of the extinction-to-backscatter ratios and the random error due to the definition of the normalisation height, was estimated at 11% (Schenkels, 2018).

Daily averaged retrievals were compared for cloud free periods for each instrument. Since the instruments were not in the same position, the cloud-free periods can differ. However, the AOT distribution is assumed to be spatially consistent on the spatial scale of around 6 km. The comparison is shown in Fig. 7. The comparsion between the AERONET and lidar retrieved AOT is good, the correlation coefficient was 0.76 (not shown). Unfortunately, on 25 and 26 September 2016 the lidar was not operational, while AERONET showed elevated AOT values on those days.

5.2 Cloud parameters

To validate the cloud retrievals from the UV-polarisation lidar, cloud radars located on the ARM Research Facility were used.

In 2016, a W-band Scanning ARM Cloud Radar (WSACR) was operated from the start of the lidar measurement period until 11 September. In 2017, a KA-band Scanning ARM Cloud Radar (KASACR) was operated during the entire period of the lidar operation. WSACR was operated at a frequency of 94 GHz and KaSACR at 35.3 GHz. Both radars have a field of view of 0.3 degrees. Although the radars were operated with scanning strategies, here only the vertical pointing modes were used, taken each hour for a duration of 4 minutes. The 2D radar reflectivity factor Z, with a time resolution of 2 s and a vertical resolution of 30 m, was collected from the ARM website.

The radar reflectivity was used to derive R_{eff}^{100} following the method described by Frisch et al. (1995): Assuming a cloud with a lognormal droplet size distribution

$$n(r) = \frac{N_d}{\sqrt{2\pi} r \sigma_x} \exp\left(\frac{-(\ln(r) - \ln(R_0))^2}{2\sigma_x^2}\right), \tag{16}$$

where is R_0 the median radius and σ_x the spread of the lognormal distribution, the effective cloud droplet radius R_{eff} is related to the median radius by

$$R_{\text{eff}} = R_0 \exp(\frac{5}{2}\sigma_x^2), \tag{17}$$

and the radar reflectivity is

$$Z = 2^6 N_d R_0^6 \exp(18\sigma_x^2). \tag{18}$$

This gives a relationship for the effective cloud droplet radius

$$R_{\text{eff}} = \frac{1}{2}\left(\frac{Z}{N_d}\right)^{1/6} \exp(-0.5\sigma_x^2). \tag{19}$$

https://doi.org/10.5194/acp-2022-473
Preprint. Discussion started: 28 July 2022


Atmospheric Chemistry and Physics Discussions

It is clear that relatively large changes in N_d or σ_x will produce only small changes in R_{eff}. The value for σ_x was set to 0.34 ± 0.09, which is a typical value for marine, low-level stratocumulus clouds (Fairall et al., 1990; Frisch et al., 1995; Miles et al., 2000). A typical value for N_d for marine, low-level stratocumulus clouds is 100 ± 70 cm^3 (Davidson et al., 1984; Martin et al., 1994). Additionally, N_d can also be estimated from the lidar inversions (see Eq. (11)). Daily averaged values of N_d were also used to estimate R_{eff}. The error margins were used to compute the uncertainty in the method using an uncertainty of $\pm$ 3 dBZ in the reflectivity factor.

R_{eff}^{100} estimates from lidar and cloud radar are compared in Figs. 8 and 9. The top panels show the lidar retrieval for selected cloud periods, with the variance in the cloud shown by error bars and the estimated measurement error shown by the shaded grey area. The average retrieved effective droplet radius is shown by the green dashed line and was $3.63 \pm 0.5\mu$m in 2016 and 3.37 ± 0.4 in 2017. The bottom panels show the R_{eff}^{100} retrieval from the cloud radar in red using the constant value for N_d and for a daily varying N_d from lidar in grey. In general, the estimates of R_{eff}^{100} from the cloud radar are larger than from the lidar, especially for a constant N_d value. Using a daily varying estimate for N_d from the lidar gives slightly more consistent estimates, which is due to the larger N_d estimate from the lidar. On average, daily lidar estimates of N_d were around 466 ± 127 cm^{-3} in 2016 and 540 ± 142 cm^{-3} in 2017. This is significantly higher than the value of 100 cm^{-3} from the literature, and a larger cloud droplet concentration will reduce the effective cloud droplet size estimate.

A dependence on N_d can be removed altogether using cloud liquid water path (LWP) data from a microwave radiometer (MWR) (Frisch et al., 2002). An MWR was operated at 23.8 and 31.4 GHz on the ARM site in 2016, but only until 11 September 2016. R_{eff}^{100} was also derived using the MWR and compared. The LWP measurements yielded much wildly varying R_{eff}^{100} than both the lidar retrievals and radar retrieval shown in Fig. 8. However, a proper comparison was difficult due to the low number of measurements from the MWR, and it was not established whether the differences were due to possible drizzle contamination or problems in the MWR data or something else. Details can be found in Schenkels (2018).

The reason for the discrepancy between the different methods is difficult to determine, since all are sensitive to assumptions. The large difference suggests that the determination of even one key parameter like the number density is highly uncertain. The lidar retrieval of this parameter was more than 5 times higher than the assumed 100 g m^{-2}, yielding low estimates of the effective cloud droplet radius.

Clearly, the lidar retrievals are much lower than those from the radar. Since all instruments and methods suffer from large uncertainties, it is hard to establish the most accurate retrieval. Cloud droplet radii are strongly dependent on the height in the cloud, growing with altitude. The UV lidar beam will never reach very far into the cloud due to its short wavelength, while the radar beam will easily penetrate a stratocumulus deck entirely. Although the lower parts of the clouds have been analysed, it cannot be ruled out that the radar senses particles from higher up in the cloud than the lidar. Furthermore, radar measurements are more sensitive to drizzle contamination than lidar measurements, and drizzle may have affected the results.

5.3 Cloud Base Height validaton

The effective radius was determined at a reference of 100 m above cloud base height (CBH), which was related to the peak of the observed parallel lidar attenuated backscatter. It is important to compare the cloud parameters from the lidar and the cloud

https://doi.org/10.5194/acp-2022-473
Preprint. Discussion started: 28 July 2022


Atmospheric Chemistry and Physics Discussions

radars at the same relative height, since the effective radius strongly depends on the height in the cloud (Zhang et al., 2011). The accuracy of the backscatter peak as the CBH cannot directly be compared to the CBH from the cloud radar, because of the different locations of the instrument. The effect of the spatial distance between the instruments was investigated by comparing CBH from two ceilometers that were installed in the airport and the ARM main site. The CBH from these instruments, relative to the mean sea level, are highly correlated in general. However, on average a higher cloud fraction was found over the main ARM site compared to the airport, due to the higher elevation of the site. This is illustrated in Fig. 10 for one day, 26 August 2017. More low-level clouds were detected over the ARM main site and the cloud fraction differed. However, this should not affect the analyses too much, since the main difference is in the low-level clouds and the selected cloud periods had CBH's higher than 1000 m.

The CBH from the lidar and from the ceilometer at the airport were compared, as shown in Fig. 11. The correlation was higher than 90%. Therefore, the relative height of the peak of the backscatter can be considered a good proxy for the relative position of the CBH.

6 Conclusions

In this paper the first indirect or Twomey effect is shown for periods of smoke incursions in stratocumulus clouds around Ascension Island, a remote island in the south-east Atlantic ocean, using a single instrument, a UV-polarisation lidar. Lidar measurements have a long history of retrieving aerosol extinction and backscatter profiles, and aerosol optical thickness in clear sky scenes. In clouds, the relationship between the return signal and the photon travel time is lost, and the lidar beam becomes inscreasingly depolarised, due to multiple scattering. In this study, the measured depolarisation of the lidar beam is fitted to LUTs of precalculated depolarisation by cloud droplets using Monte Carlo (MC) simulations, relating the depolarisation to cloud droplet effective radius and the cloud extinction parameter at a reference height. This can be used to study both aerosol optical thickness and cloud parameters changes using a single instrument. A UV-polarisation lidar, normally located in Cabauw, The Netherlands, was installed on Ascension Island during one month in 2016 and one month in 2017, to study stratocumulus cloud droplet size and number density in relationship with aerosol optical thickness. Over Ascension, smoke from vegetation fires in Africa is often observed during the African dry season, which is about July to September.

In this study, we found indications of the first indirect effect in clouds over Ascension during days when smoke was found at cloud level during cloud-free periods, compared to days when the air was smoke-free at the cloud level during cloud-free periods. On average, the cloud drop number density was 294 ± 91 cm^3 and cloud effective radius 3.81 ± 0.6 μm during smoke free days, compared to 611 ± 191 cm^3 and 2.85 ± 0.2 μm during days with smoke at cloud level.

Similarly, when the cloud parameters during cloud periods were related to the daily averaged AOT at cloud level (300 m below cloud base to 1000 m above cloud base) an indirect effect was found: 0.3 ± 0.21 cm^{-3} for the cloud droplet number density and 0.18 ± 0.06 μm for the cloud effective radius.

Lastly, by solving the Klett-Fernald boundary value problem within the cloud, where the aerosol extinction is negliglible compared to the cloud extinction, the aerosol and cloud properties were retrieved simultaneously by the lidar. In this case, the

https://doi.org/10.5194/acp-2022-473
Preprint. Discussion started: 28 July 2022


Atmospheric Chemistry and Physics Discussions

average aerosol extinction below the cloud was taken as the aerosol proxy, because the profile heights differed, which would lead to different AOT delepending on the height over which was integrated. The resulting indirect effect picture is difficult to interpret due to the large uncertainties, but from 12–15 Aug. 2016 and 20–24 Aug. 2016 an indirect effect was found. These periods correspond to the days that smoke was found at the cloud layer and in the free troposphere.

The lidar aerosol and cloud parameter retrievals were compared to retrievals using different instruments installed on the island. The AOT from the lidar corresponds well to 340 nm AERONET AOT retrievals during cloud-free periods, even though the AERONET sunphotometer was 6 km from the lidar.

The cloud effective radius retrieval from the MC multiple scattering simulation retrievals were compared to cloud effective radii retrieved using cloud radars installed on the ARM main site. The distance of 6 km between the instruments has a noticeable effect on the cloud fraction above the instruments: Over the ARM main site the cloud fraction is generally higher, due to more low lying clouds over this site. However, this should not effect the analysis of the cloud parameter comparison much, since only clouds with a CBH above 1000 m were used in the analyses.

The cloud effective radii from the lidar were smaller than those from the cloud radar, in all years and using several methods for the radar retrievals. $R^1 00_{\text{eff}}$ retrieved by the lidar was $3.63 \pm 0.5 \mu$m on average in 2016, $R^1 00_{\text{eff}}$ retrieved by the radar was $7.49 \pm 2.52 \mu$m for a constant cloud droplet number concentration N_d taken from literature. If N_d was estimated from the lidar measurements, the cloud effective radius retrieved by the radar became $5.8 \pm 2.0 \mu$m and more consistent with the lidar retrieval. An attempt to remove the dependence on N_d altogether by using LWP from a MWR did not give any conclusive results.

Note that cloud droplet size is highly dependent on height, growing with altitude. The lidar beam at 355 nm never penetrates deep into the cloud, we estimate it to be confined to 100-300 m above CBH. The radar on the other hand travels far into the cloud and can even retrieve the cloud properties at the top of a stratocumulus deck. Care has been taken to retrieve the cloud parameters at the lower parts of the clouds, but it cannot be ruled out that the radar is more sensitive to signals from higher up in the cloud than the lidar. Furthermore, drizzle contamination of the radar retrievals cannot be ruled out.

The cloud effective radius retrieval is the most uncertain parameter in the analyses. It is unclear which retrieval of the cloud effective radius is most reliable, since all methods and instruments suffer from large uncertainties. The lidar has been a valuable tool to study aerosol parameter profiles. This study shows the suitability to also study cloud effective radius using depolarisation from the lidar beam. This can help to reduce the uncertainty in cloud effective radius retrievals by independent measurements. Furthermore, the simultaneous retrievals of aerosol extinction and cloud properties from one single instrument can be instrumental in the measurement of aerosol indirect effects, which constitutes the largest uncertainties in global climate models.

Data availability. The data acquired on Ascension Island by the UV-polarisation lidar are freely available.

https://doi.org/10.5194/acp-2022-473
Preprint. Discussion started: 28 July 2022

Atmospheric Chemistry and Physics Discussions

Author contributions. MdG authored the science application, coordinated and managed the measurement campaigns, and wrote the paper; KS co-authored the science application; JB performed the 2016 measurements; ET analysed the 2016 data; MS performed and analysed the 2017 data; DD designed the MS model, calibrated the UV-lidar and overlooked the science.

Competing interests. None

Acknowledgements. This project was financed by the Pieter Langerhuizen Stipedium of the Koninklijke Hollandsche Maatschappij der Wetenschappen (http://www.khmw.nl/ in Haarlem, The Netherlands, supplemented with financial support from TUD and manpower from TUD, KNMI and WUR, for which we are greatly indebted. We are also grateful for the support of the RAF personnel and staff at Wideawake airfield. Special thanks go to Prof. Jim Haywood from the UK Met Office and Exeter U. for his leadership and help on numerous occasions of logistics mayhem, and Jenna Macgregor of the Ascension Island Met Office for her initiatives and help on the Ascension side.

https://doi.org/10.5194/acp-2022-473
Preprint. Discussion started: 28 July 2022

Atmospheric Chemistry and Physics Discussions

References

Brown, J.: Inverting ground-based polarisation lidar measurements to retrieve cloud microphysical properties during the Ascension Island Initiative, Internship report KNMI IR-2016-10, Royal Netherlands Meteorological Institute (KNMI) and WUR, https://cdn.knmi.nl/knmi/pdf/bibliotheek/knmipubIR/IR2016-10.pdf, 2016.

Cattrall, C., Reagan, J., Thome, K., and Dubovik, O.: Variability of aerosol and spectral lidar and backscatter and extinction ratios of key aerosol types derived from selected Aerosol Robotic Network locations, Journal of Geophysical Research: Atmospheres, 110, n/a–n/a, https://doi.org/10.1029/2004JD005124, d10S11, 2005.

Collis, R. T. H. and Russel, P. B.: Lidar measurement of particles and gases by elastic backscattering and differential absorption, in: Laser monitoring of the atmosphere. Topics in Applied Physics, vol 14., edited by Hinkley, E. D., chap. 4, pp. 71–151, Springer, Berlin Heidelberg, https://doi.org/10.1007/3-540-07743-X_18, 1976.

Davidson, K. L., Fairall, C. W., Boyle, P. J., and Schacher, G. E.: Verification of an Atmospheric Mixed-Layer Model for a Coastal Region, Journal of Climate and Applied Meteorology, 23, 617–636, https://doi.org/10.1175/1520-0450(1984)023<0617:VOAAML>2.0.CO;2, 1984.

de Roode, S. R. and Los, A.: The effect of temperature and humidity fluctuations on the liquid water path of non-precipitating closed-cell stratocumulus clouds, Quarterly Journal of the Royal Meteorological Society, 134, 403–416, https://doi.org/10.1002/qj.222, 2008.

Donovan, D. P., Klein Baltink, H., Henzing, J. S., de Roode, S. R., and Siebesma, A. P.: A depolarisation lidar-based method for the determination of liquid-cloud microphysical properties, Atmos. Meas. Tech., 8, 237–266, https://doi.org/10.5194/amt-8-237-2015, 2015.

Dorman, C. E. and Bourke, R. H.: Precipitation over the Atlantic Ocean, 30°S to 70°N, Monthly Weather Review, 109, 554–563, https://doi.org/10.1175/1520-0493(1981)109<0554:POTAOT>2.0.CO;2, 1981.

Eck, T. F., Holben, B. N., Reid, J. S., Dubovik, O., Smirnov, A., O'Neill, N. T., Slutsker, I., and Kinne, S.: Wavelength dependence of the optical depth of biomass burning, urban, and desert dust aerosols, Journal of Geophysical Research: Atmospheres (1984–2012), 104, 31 333–31 349, https://doi.org/10.1029/1999JD900923, 1999.

Fairall, C. W., Hare, J. E., and Snider, J. B.: An Eight-Month Sample of Marine Stratocumulus Cloud Fraction, Albedo, and Integrated Liquid Water, Journal of Climate, 3, 847–864, https://doi.org/10.1175/1520-0442(1990)003<0847:AEMSOM>2.0.CO;2, 1990.

Feingold, G., Remer, L. A., Ramaprasad, J., and Kaufman, Y. J.: Analysis of smoke impact on clouds in Brazilian biomass burning regions: An extension of Twomey's approach, J. Geophys. Res., 106, 22 907–22 922, https://doi.org/https://doi.org/10.1029/2001JD000732, 2001.

Fernald, F. G.: Analysis of atmospheric lidar observations: some comments, Appl. Opt., 23, 652–653, https://doi.org/10.1364/AO.23.000652, 1984.

Formenti, P., D'Anna, B., Flamant, C., Mallet, M., Piketh, S. J., Schepanski, K., Waquet, F., Auriol, F., Brogniez, G., Burnet, F., Chaboureau, J.-P., Chauvign?, A., Chazette, P., Denjean, C., Desboeufs, K., Doussin, J.-F., Elguindi, N., Feuerstein, S., Gaetani, M., Giorio, C., Klopper, D., Mallet, M. D., Nabat, P., Monod, A., Solmon, F., Namwoonde, A., Chikwililwa, C., Mushi, R., Welton, E. J., and Holben, B.: The Aerosols, Radiation and Clouds in Southern Africa Field Campaign in Namibia: Overview, Illustrative Observations, and Way Forward, Bulletin of the American Meteorological Society, 100, 1277 – 1298, https://doi.org/10.1175/BAMS-D-17-0278.1, 2019.

Frisch, A. S., Fairall, C. W., and Snider, J. B.: Measurement of Stratus Cloud and Drizzle Parameters in ASTEX with a Ka-Band Doppler Radar and a Microwave Radiometer, Journal of the Atmospheric Sciences, 52, 2788–2799, https://doi.org/10.1175/1520-0469(1995)052<2788:MOSCAD>2.0.CO;2, 1995.

https://doi.org/10.5194/acp-2022-473
Preprint. Discussion started: 28 July 2022

Atmospheric Chemistry and Physics Discussions

Frisch, A. S., Shupe, M., Djalalova, I., Feingold, G., and Poellot, M.: The Retrieval of Stratus Cloud Droplet Effective Radius with Cloud Radars, Journal of Atmospheric and Oceanic Technology, 19, 835–842, https://doi.org/10.1175/1520-0426(2002)019<0835:TROSCD>2.0.CO;2, 2002.

Greatwood, C., Richardson, T., Freer, J., Thomas, R., Rob Mackenzie, A., Brownlow, R., Lowry, D., Fisher, R., and Nisbet, E.: Atmospheric sampling on ascension island using multirotor UAVs, Sensors, 17, 1–24, https://doi.org/10.3390/s17061189, 2017.

Guzzi, R.: Exploring the Atmosphere by Remote Sensing Techniques, Lecture Notes in Physics, Springer Berlin Heidelberg, httpfs://books.google.nl/books?id=RPRpCQAAQBAJ, 2008.

Haywood, J. M., Abel, S. J., Barrett, P. A., Bellouin, N., Blyth, A., Bower, K. N., Brooks, M., Carslaw, K., Che, H., Coe, H., Cotterell, M. I., Crawford, I., Cui, Z., Davies, N., Dingley, B., Field, P., Formenti, P., Gordon, H., de Graaf, M., Herbert, R., Johnson, B., Jones, A. C., Langridge, J. M., Malavelle, F., Partridge, D. G., Peers, F., Redemann, J., Stier, P., Szpek, K., Taylor, J. W., Watson-Parris, D., Wood, R., Wu, H., and Zuidema, P.: The CLoud–Aerosol–Radiation Interaction and Forcing: Year 2017 (CLARIFY-2017) measurement campaign, Atmospheric Chemistry and Physics, 21, 1049–1084, https://doi.org/10.5194/acp-21-1049-2021, 2021.

Kim, J.-H., Schneider, R. R., Mulitza, S., and Müller, P. J.: Reconstruction of SE trade-wind intensity based on sea-surface temperature gradients in the Southeast Atlantic over the last 25 kyr, Geophys. Res. Lett., 30, https://doi.org/https://doi.org/10.1029/2003GL017557, 2003.

Klett, J. D.: Stable analytical inversion solution for processing lidar returns, Appl. Opt., 20, 211–220, https://doi.org/10.1364/AO.20.000211, 1981.

Liou, K.-N. and Schotland, R. M.: Multiple Backscattering and Depolarization from Water Clouds for a Pulsed Lidar System, Journal of the Atmospheric Sciences, 28, 772–784, https://doi.org/10.1175/1520-0469(1971)028<0772:MBADFW>2.0.CO;2, 1971.

Martin, G. M., Johnson, D. W., and Spice, A.: The Measurement and Parameterization of Effective Radius of Droplets in Warm Stratocumulus Clouds, Journal of the Atmospheric Sciences, 51, 1823–1842, https://doi.org/10.1175/1520-0469(1994)051<1823:TMAPOE>2.0.CO;2, 1994.

Miles, N. L., Verlinde, J., and Clothiaux, E. E.: Cloud Droplet Size Distributions in Low-Level Stratiform Clouds, Journal of the Atmospheric Sciences, 57, 295–311, https://doi.org/10.1175/1520-0469(2000)057<0295:CDSDIL>2.0.CO;2, 2000.

Müller, D., Ansmann, A., Mattis, I., Tesche, M., Wandinger, U., Althausen, D., and Pisani, G.: Aerosol-type-dependent lidar ratios observed with Raman lidar, Journal of Geophysical Research: Atmospheres, 112, n/a–n/a, https://doi.org/10.1029/2006JD008292, d16202, 2007.

Redemann, J., Wood, R., Zuidema, P., Doherty, S. J., Luna, B., LeBlanc, S. E., Diamond, M. S., Shinozuka, Y., Chang, I. Y., Ueyama, R., Pfister, L., Ryoo, J., Dobracki, A. N., da Silva, A. M., Longo, K. M., Kacenelenbogen, M. S., Flynn, C. J., Pistone, K., Knox, N. M., Piketh, S. J., Haywood, J. M., Formenti, P., Mallet, M., Stier, P., Ackerman, A. S., Bauer, S. E., Fridlind, A. M., Carmichael, G. R., Saide, P. E., Ferrada, G. A., Howell, S. G., Freitag, S., Cairns, B., Holben, B. N., Knobelspiesse, K. D., Tanelli, S., L'Ecuyer, T. S., Dzambo, A. M., Sy, O. O., McFarquhar, G. M., Poellot, M. R., Gupta, S., O'Brien, J. R., Nenes, A., Kacarab, M. E., Wong, J. P. S., Small-Griswold, J. D., Thornhill, K. L., Noone, D., Podolske, J. R., Schmidt, K. S., Pilewskie, P., Chen, H., Cochrane, S. P., Sedlacek, A. J., Lang, T. J., Stith, E., Segal-Rozenhaimer, M., Ferrare, R. A., Burton, S. P., Hostetler, C. A., Diner, D. J., Platnick, S. E., Myers, J. S., Meyer, K. G., Spangenberg, D. A., Maring, H., and Gao, L.: An overview of the ORACLES (ObseRvations of Aerosols above CLouds and their intEractionS) project: aerosol-cloud-radiation interactions in the Southeast Atlantic basin, Atmos. Chem. Phys. Disc., 2020, 1–82, https://doi.org/10.5194/acp-2020-449, 2020.

Rodgers, C.: Inverse Methods for Atmospheric Sounding: Theory and Practice, Series on atmospheric, oceanic and planetary physics, World Scientific, https://books.google.nl/books?id=FjxqDQAAQBAJ, 2000.

https://doi.org/10.5194/acp-2022-473
Preprint. Discussion started: 28 July 2022

Atmospheric Chemistry and Physics Discussions

Sarna, K., Donovan, D. P., and Russchenberg, H. W. J.: Estimating optical extinction of liquid water clouds in the cloud base region, Atmos. Meas. Tech., 14, 4959–4970, https://doi.org/10.5194/amt-14-4959-2021, 2021.

Sassen, K. and Petrilla, R. L.: Lidar depolarization from multiple scattering in marine stratus clouds, Appl. Opt., 25, 1450–1459, https://doi.org/10.1364/AO.25.001450, 1986.

Schenkels, M.: Aerosol Optical Depth and Cloud Parameters from Ascension Island retrieved with a UV-depolarisation Lidar: An outlook on the validation, Master thesis KNMI TR-366, Royal Netherlands Meteorological Institute (KNMI) and UU, https://studenttheses.uu.nl/handle/20.500.12932/30472, 2018.

Tenner, E. V.: The UV-LIDAR: A tool for investigating Aerosol-Cloud Interactions: A case study on Ascension Island, Master thesis, Delft University of Technology, http://resolver.tudelft.nl/uuid:2fa8eb2d-3523-4611-a006-7aa5f52e8ecd, 2017.

Twomey, S. A.: The Influence of Pollution on the Shortwave Albedo of Clouds, J. Atmos. Sci., 34, 1149–1152, 1977.

Wandinger, U., Baars, H., Engelmann, R., Hünerbein, A., Horn, S., Kanitz, T., Donovan, D., van Zadelhoff, G.-J., Daou, D., Fischer, J., von Bismarck, J., Filipitsch, F., Docter, N., Eisinger, M., Lajas, D., and Wehr, T.: HETEAC: The Aerosol Classification Model for EarthCARE, EPJ Web of Conferences, 119, 01 004, https://doi.org/10.1051/epjconf/201611901004, 2016.

Zhang, S., Xue, H., and Feingold, G.: Vertical profiles of droplet effective radius in shallow convective clouds, Atmospheric Chemistry and Physics, 11, 4633–4644, 2011.

Zuidema, P., Redemann, J., Haywood, J., Wood, R., Piketh, S., Hipondoka, M., and Formenti, P.: Smoke and Clouds above the Southeast Atlantic: Upcoming Field Campaigns Probe Absorbing Aerosol's Impact on Climate, Bull. Am. Meteor. Soc., 97, 1131–1135, https://doi.org/10.1175/BAMS-D-15-00082.1, 2016.

https://doi.org/10.5194/acp-2022-473
Preprint. Discussion started: 28 July 2022

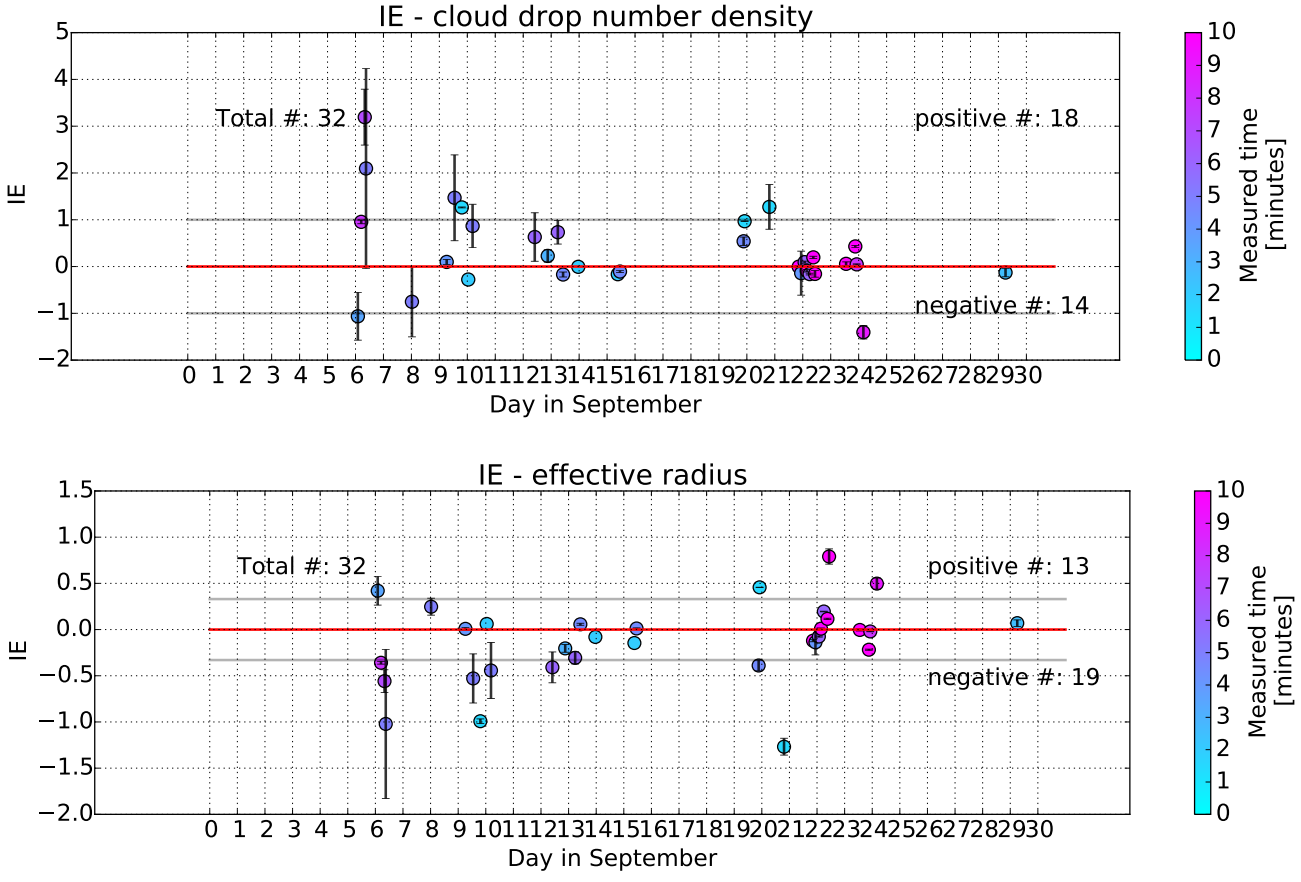

Figure 6. Indirect Effect (IE) for each selected cloud period in Sept. 2016, using the average aerosol extinction profile below a cloud and the retrieved cloud droplet number density (top) and the retrieved cloud droplet effective radius (bottom). The error bars indicate the standard deviation of the measurements during each selected interval, the colors indicate the duration of the intervals. The grey horizontal lines indicate the physically feasible bounds of the IE values.

https://doi.org/10.5194/acp-2022-473
Preprint. Discussion started: 28 July 2022

Atmospheric Chemistry and Physics Discussions

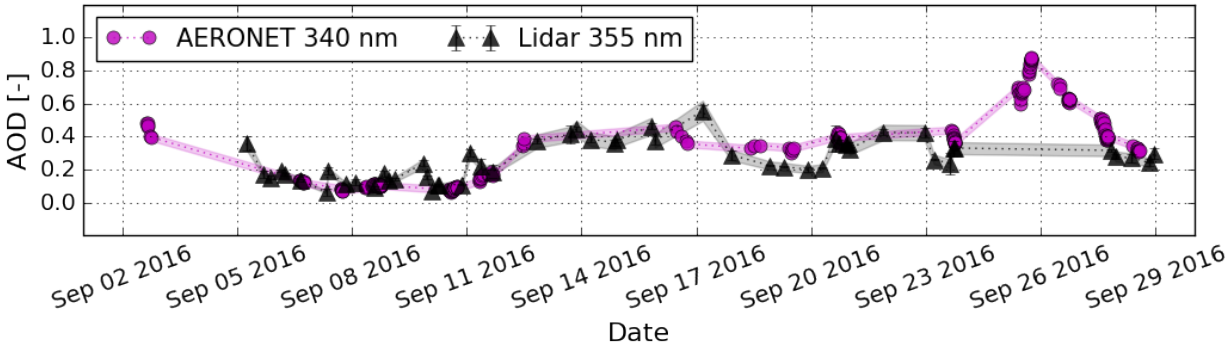

Figure 7. Aerosol Optical Thickness retrievals from AERONET at 340 nm (purple) compared to the retrieval from the UV-lidar at 355 nm (grey). The black error bars show the standard deviation of the lidar retrievals. The shaded areas indicate the retrieval uncertainties, 0.021 for AERONET AOT (light purple) and 11% for the lidar data (light grey).

https://doi.org/10.5194/acp-2022-473
Preprint. Discussion started: 28 July 2022

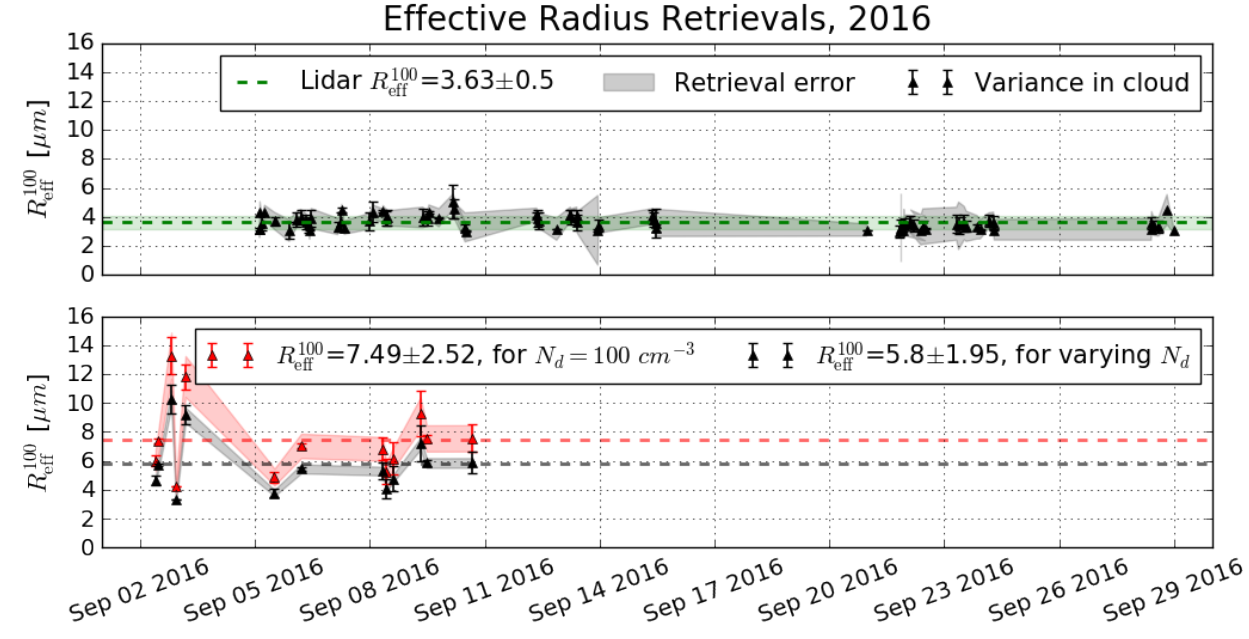

Figure 8. R_{eff}^{100} for selected cloud periods in 2016 from (a) lidar and (b) cloud radar. The shading shows the standard deviation or retrieval error, while the variance in the cloud per measurement period is given by the error bars. The dashed line gives the mean R_{eff}^{100}. In (b) the red measurements are obtained using a constant N_d, while the grey measurements were obtained using a lidar derived N_d.

https://doi.org/10.5194/acp-2022-473
Preprint. Discussion started: 28 July 2022

Atmospheric Chemistry and Physics Discussions

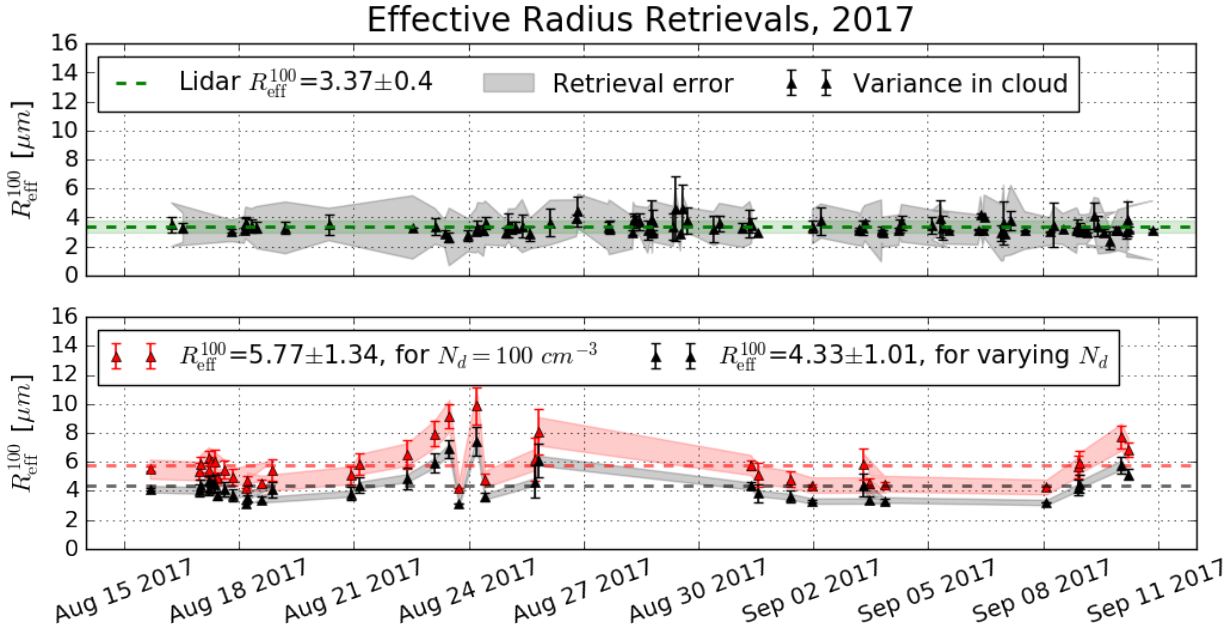

Figure 9. R_{eff}^{100} for selected cloud periods in 2017 from (a) lidar and (b) cloud radar. The shading shows the standard deviation or retrieval error, while the variance in the cloud per measurement period is given by the error bars. The dashed line gives the mean R_{eff}^{100}.

https://doi.org/10.5194/acp-2022-473
Preprint. Discussion started: 28 July 2022

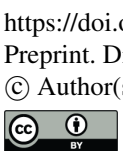

Atmospheric Chemistry and Physics Discussions

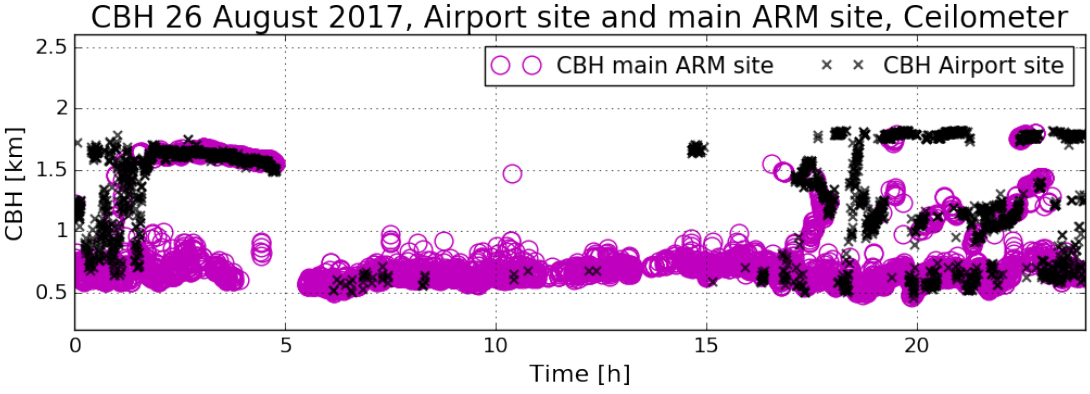

Figure 10. The CBH from the ceilometer at the airport (black crosses) compared to the CBH from the Ceilometer at the main ARM site (purple circles) on 26 August 2017. The CBH is measured relative to the mean sea level.

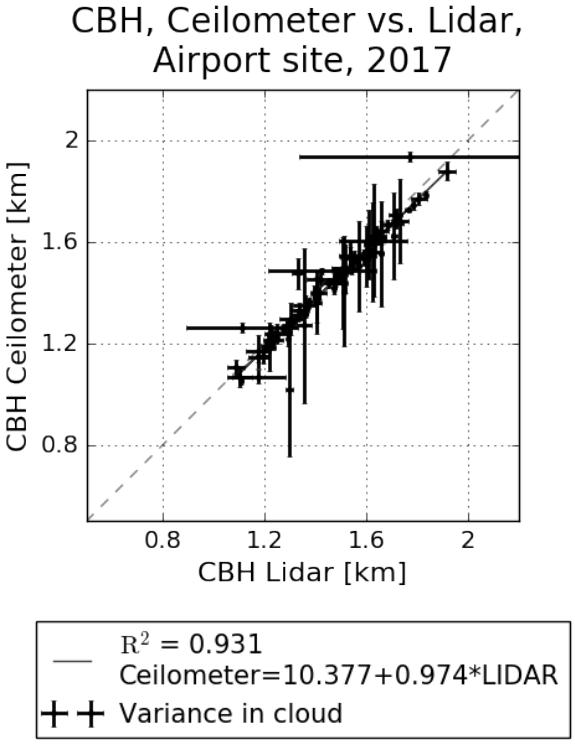

Figure 11. Comparison of the cloud base height determined from the UV-lidar and the ceilometer located on the airport.